Tuning of photoluminescence intensity and Fermi level position of individual single-walled carbon nanotubes by molecule confinement

Romain Chambard, Juan Carlos Moreno-López, Patrick Hermet, Yuta Sato, Kazu Suenaga, Thomas Pichler, Bruno Jousselme, Raymond Aznar, Jean-Louis Bantignies, Nicolas Izard, et al.

Tuning of photoluminescence intensity and Fermi level position of individual single-walled carbon nanotubes by molecule confinement

Romain Chambard [a], Juan-Carlos Moreno-Lopez [b], Patrick Hermet [c] Yuta Sato [d], Kazu Suenaga [e], Thomas Pichler, [b] Bruno Jousselme [f], Raymond Aznar [a], Jean-Louis Bantignies [a], Nicolas Izard [a], Laurent Alvarez [a*]

[a] Laboratoire Charles Coulomb (L2C), CNRS-University of Montpellier, Montpellier, France

[b] Faculty of Physics, University of Vienna, Boltzmanngasse 5, 1090, Vienna, , Austria

[c] Institut Charles Gerhardt Montpellier, CNRS-UM-ENSCM, Montpellier, France

[d] Nanomaterials Research Institute, National Institute of Advanced Industrial Science and Technology (AIST), Tsukuba, 305-8565, Japan

[e] The Institute of Scientific and Industrial Research (ISIR), Osaka University, Osaka 567-0047, Japan

[f] Université Paris-Saclay, CEA, CNRS, NIMBE, LICSEN, Gif-sur-Yvette, 91191, France

* corresponding author : laurent.alvarez@umontpellier.fr

ABSTRACT: Photoluminescence of single-walled carbon nanotubes is monitored at the individual scale by molecule encapsulation into their hollow core. Depending on the electronic character (electron donor or acceptor) of the confined molecule, enhancement or quenching of the photoluminescence intensity is demonstrated. This behavior is assigned to a charge transfer, evidenced by the shift of the Raman G-band, and a correlated Fermi level shift shown by photoemission experiments. Our experimental results are supported by DFT calculations. A consistent picture of the physical interactions taking place in the hybrid systems and their effects on the optical and electronic properties is given. Our results indicate that the electron affinity or ionization potential of the encapsulated molecules and the diameter of the nanotube are relevant parameters to tune the light emission properties of the hybrid systems at the nanoscale.

KEYWORDS: Individual Nanotube, photoluminescence, Raman, photoemission.

1. Introduction

Carbon based nanostructures as single-walled carbon nanotubes (NT) opened new opportunities for electronics[1–3] and photonics[4–6]. However, their theoretical outstanding opto-electronic properties are hampered by their local environment [7–9] or defects.[10] Therefore, controlling the adsorption at the inner surface of NT is of most importance to master their properties. Filling the hollow core of NT with molecules [11–18] is an efficient way to control and even improve the NT properties by properly choosing the confined species.[13,14,16,18–24] Encapsulation of specific molecules can activate non-linear optical response,[13] modify the photoluminescence (PL) intensity,[14,19] tune the absorbance window,[21] photo-activate charge transfer (CT),[22] shift the Fermi level[14,23] or significantly enhance the Raman response.[16] The physical parameters most often used to tune the properties are the dielectric constant of the molecule, [19] the supramolecular organization,[12,13,16] or the electrochemical doping.[25] The amphoteric character of NT, combined to electron donor or acceptor molecule in order to create a charge transfer complex with new and tailored opto-electronic properties has been only qualitatively studied.[14,18,22]

In this article, we investigate the optoelectronic properties of narrow diameter NT (d~0.9 nm) in which electron donor -quaterthiophene (4T) and tetramethyl-*p*-phenylenediamine (TMPD)- or acceptor -tetrafluoro-tetracyanoquinodimethane (F_4TCNQ) and tetracyano-quinodimethane (TCNQ)- molecules are confined into their hollow core.

Enhancement or quenching of the PL intensities are clearly evidenced and correlated to an electron or hole transfer to the host NT, shifting the Fermi level. A very good correlation between the photoluminescence intensity modifications, the charge transfer and the Fermi level shifts is evidenced. Therefore, with the significant improvement in the chirality-pure NT preparation,[26] molecule encapsulation allows tailoring the light emission properties of the hybrid systems at the nanoscale.

2. Materials and Methods :

2.1 Sample preparation: 7,7,8,8-Tetracyanoquinodimethane (TCNQ), 2,3,5,6-Tetrafluoro-7,7,8,8-tetracyanoquinodimethane (F_4TCNQ) and N,N,N′,N′-Tetramethyl-p-phenylenediamine (TMPD) were purchased from Aldrich and used as received. 5,5”’-Dimethyl-2,2’:5’,2”:5”,2”’-tetrathiophene (4TCH3) were prepared according to following described procedure:[27] the

targeted compound 5,5"'-Dimethyl-2,2':5',2":5",2"'-tetrathiophene (4T) was synthesized using Grignard coupling between the 2-Bromo-5-methylthiophene and the 5,5'-Dibromo-2,2'-bithiophene molecules in the presence of palladium catalyst. All reagents and chemicals were purchased from Sigma-Aldrich.

The source of NT are as received NT from Sigma Aldrich and consists in CoMoCAT carbon nanotubes[28] (0.7 nm< d < 1 nm), purified and enriched in (7,6) nanotube. The hybrid nanotubes with 4T, TMPD, TCNQ and F_4TCNQ are labelled 4T@NT, TMPD@NT, TCNQ@NT and F_4TCNQ@NT in the following. Those molecules are chosen regarding their ionization energy and electron affinity.[29] Moreover, those molecules exhibit low sublimation temperature around 140-170°C,[30,31] which make them good candidates for vapor encapsulation. Encapsulation of molecules into NT is performed using the vapor reaction method previously described[12,14]. NT and the molecules (M) to be confined are sealed at two different locations in a glass tube. NTs are degassed at 300°C under dynamic high vacuum (2.10^{-6} mbar) for 48H. Then NT and M are mixed in a weight ratio: w_{NT}/w_M=0.5 and heated at 250°C for 72 hour under static high vacuum. After encapsulation, a sublimation step is then performed under dynamic vacuum at 260°C to get rid of all the molecule in excess. The final sample is then washed with organic solvent and stored in the oven at 120°C for 24 hours.

The reference pristine nanotubes undergo the same thermal treatments as the hybrid sample during the encapsulation process. The powders of empty and hybrid NT are then dispersed in 1%w bile salt/water solution, with a ratio of 1mg of NT for 30 ml of solution. After being kept in ultrasonic bath, dispersion is tip sonicated for 20 minutes. The dispersion is then ultra-centrifugated (at 100 kG) for 2 hours. The upper half supernatant liquid is extracted. Concentration of the NT dispersion are then readjusted, so that all dispersion (pristine and hybrids NT dispersion) exhibit the same optical absorption band area at 660 nm, corresponding to the (7,6) nanotube absorption peaks (Figure 1, SM). The obtained solutions are then used for both absorption and macroscopic photoluminescence measurements. Finally, dispersion is spin coated on a silicon or quartz substrate with a (300 nm thick oxide). Substrates are then washed under de-ionized water, isopropanol and acetone in order to remove bile salts. These deposited nanotubes are used to perform photoluminescence and Raman measurements on isolated individual nanotubes.

2.2 Micro Raman: Micro Raman experiments are performed on individual NT deposited on substrate with a Renishaw In-Via spectrometer, using 532 and 633 nm laser diodes. Laser power under the 100X objective is set to 0.1mW to prevent heating induced band shift.

2.3 Micro Photoluminescence: Micro-PL experiment are carried out in liquid phase inside quartz cells on an ensemble of NT, or on quartz substrate for individual NT. Laser diodes at 561 nm and 660 nm are used to respectively excite (8,4) (6,5) and (8,3) (7,5) (7,6) nanotubes. Larger NT are excited in the near IR via a Ti - AL2O3 tunable laser (700-1000 nm). The spectrometer consists in Princeton Instrument Acton series 150 lines/mm grating simple monochromator. A liquid Nitrogen cooled Princeton Instrument PyLoN IR 512 pixel InGaAS array is used as detector.

Approximately 40 isolated NT are detected, and their PL spectra were investigated with the 561 and 660 nm laser excitation wavelengths. Those energies correspond to the S_{22} transition of (6,5) (8,4) and (8,3) (7,5) (7,6) nanotubes.

2.4 TEM, EELS: For Transmission Electron Microscope (TEM) and Electron Energy Loss Spectroscopy (EELS) investigation, samples (powder) are dispersed in n-hexane by ultrasonication, and dropped onto molybdenum microgrids coated with holey amorphous carbon films. A JEOL JEM-2100F electron microscope equipped with double JEOL Delta spherical aberration correctors was operated at an electron accelerating voltage of 60 kV for TEM observation. Spatially-resolved Electron energy-loss spectroscopy (SR-EELS) measurement was carried out using a Gatan Quantum electron spectrometer attached to the microscope. Elemental distributions of carbon and sulfur and nitrogen in individual NT are determined based on the intensities of their K, L and K edges, respectively, at each measured point in the scanned areas by STEM-EELS chemical mapping.

2.5 XPS/UPS: X-Ray photoelectron spectroscopy (XPS) measurements were performed with a monochromated Al Kα source (1486.5 eV) and a Scienta RS4000 analyzer with the sample grounded. The ultraviolet photoemission spectroscopy (UPS) measurements were acquired with He II (40.8eV) and the samples polarized at −6 V, to ensure that electrons emitted from the sample overcome the work function of the analyzer.

2.6 COMPUTATIONAL DETAILS: Electronic density-of-states are calculated within the formalism of the density functional theory (DFT). We use the SIESTA package[32] and the

generalized gradient approximation to the exchange correlation functional as proposed by Perdew, Burke and Ernzerhof.[33] Core electrons are replaced by nonlocal norm-conserving pseudopotentials. The valence electrons are described by a double-zeta singly polarized basis set. The localization of the basis is controlled by an energy shift of 50 meV. Real space integration is performed on a regular grid corresponding to a plane-wave cutoff of 300 Ry. Van der Waals corrections (DFT-D) between the nanotube and the molecule are considered using the semi-empirical dispersion potential parametrized by Grimme.[34] A vacuum size of 11 Å is used to avoid interactions between adjacent tubes. Atomic positions were relaxed using a conjugate gradient until the maximum residual atomic force was smaller than 0.02 eV/Å. The electronic density-of-states are obtained considering 33 *k*-points along the nanotube axis.

3. Results

3.1. Structural properties

Figure 1 displays a Scanning Transmission Microscopy (STEM) image of the hybrid F_4TCNQ@NT system.

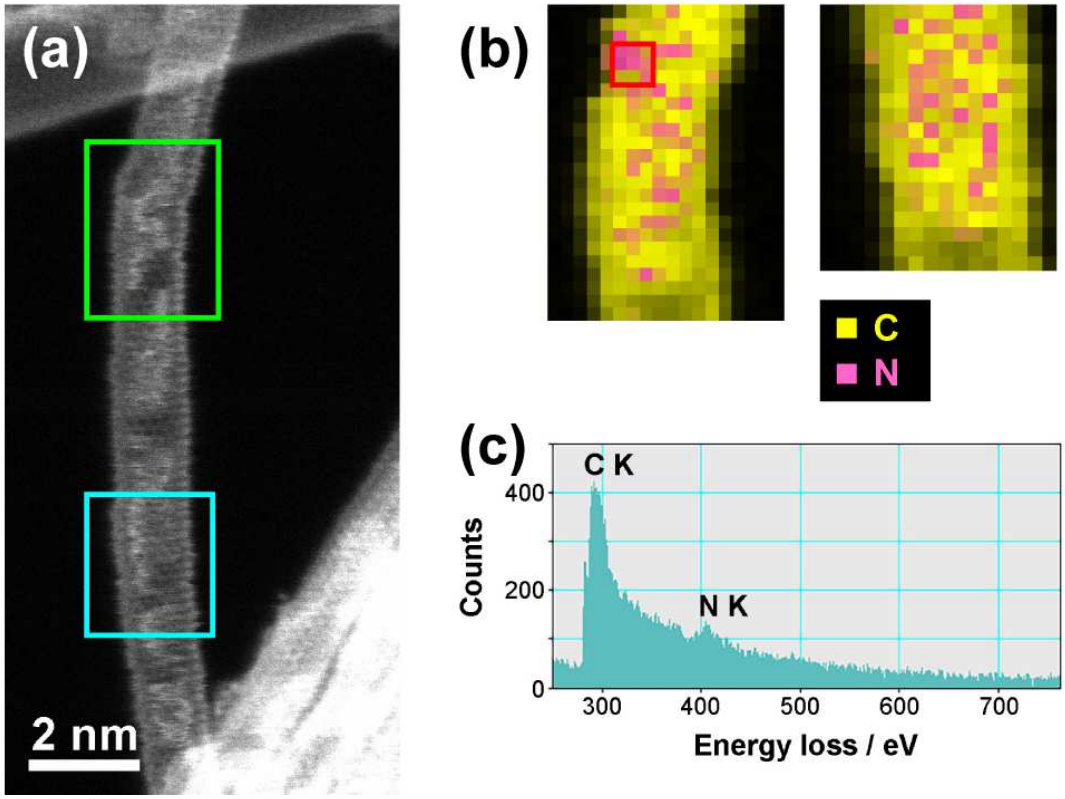

Figure 1*. (a) Annular dark-field STEM*

image of F4TCNQ@NT. (b) STEM-EELS chemical maps of carbon and nitrogen for the areas indicated by green and cyan rectangles (left and right, respectively) in (a). EEL spectrum for the area indicated by red square in (b).

The filling rate is quite good whereas no molecule is observed stacked at the outer surface of the NT, meaning that the washing steps are efficient. From EELS measurements, both the carbon and nitrogen edges are evidenced, as expected. STEM image of 4T@NT is presented in figure 2, SM.

3.2 Charge Transfer

According to the different ionization potentials (4.8 eV for NT,[35] 4.25 eV for TMPD and around 4.75 eV for 4T (estimated from the sexithiophene) [29] and electron affinities (4.2 eV for NT,[35] 4,7 eV for TCNQ and 5,24 eV for F4TCNQ[29]), significant electron or hole transfer is expected from the confined molecule to NT.

We investigate this CT from the molecule to the host NT using Raman spectroscopy. Raman spectra of individual hybrid F_4TCNQ@NT (red curve), 4T@NT (blue curve) with respect to empty NT (black curve) are displayed in figure 2. The Raman spectra of TCNQ@NT and TMPD@NT are displayed in figure 4 SM. At low frequency (200-250 cm^{-1}), the Radial Breathing Modes (RBM) are observed. We can clearly observe a decrease in the mode intensity after encapsulation, consistent with a CT which modifies the resonance conditions.[36,37] At high frequency (~1600 cm^{-1}), the spectra exhibit the G-band which is very sensitive to NT electronic properties and CT.[14,22,38–43] In both cases, we clearly observe a significant shift of the Raman G^+ band after molecule encapsulation.

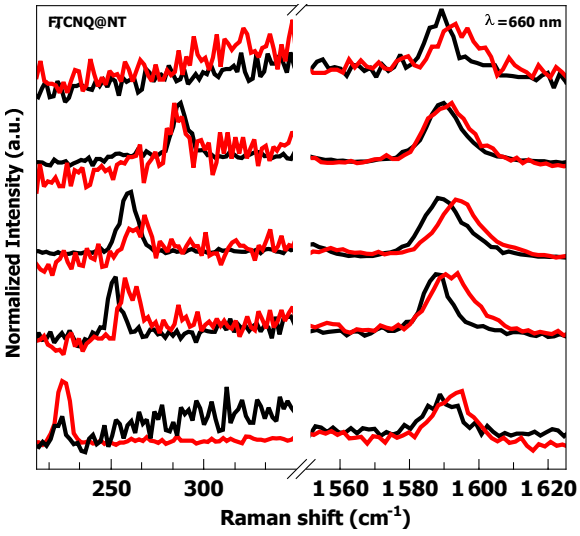

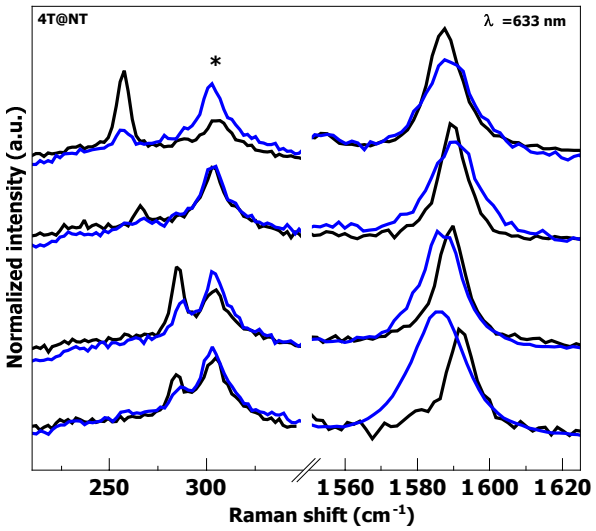

Figure 2: *Raman spectra (RBM and G-band) of 4T@NT (blue curve, λ=532 nm) deposited on a silicon substrate and F_4TCNQ@NT (red curve, λ=660 nm) deposited on a quartz substrate, with respect to empty NT (black curve).* labels a silicon Raman band. All the Raman spectra were normalized to obtain a G-band intensity equal to 1 and offset for clarity.*

This G-band shift can be assigned to a charge transfer between the confined molecules and the host NT. Indeed, the Raman G-band is expected to respectively downshift or upshift upon *n*- or *p*-type doping,[14] as observed in figure 2. For CT quantification, assuming that the G^+ band does not undergo the renormalization effect because of the too narrow NT diameter, the number of electron transferred per carbon atom of the nanotube ρ_c, can be derived by the following equation adapted from reference [44] or [38] :

$$\Delta\omega_{static}(cm^{-1}) = -804\times\rho_c - 5126\times\rho_c^2 - 176790\times\rho_c^3 - 1657\times\rho_c^{3/2} \quad (1)$$

Taking into account the lengths of the different molecules and calculating the number of carbon atoms in a NT of the same length with a diameter of 9 Å, one can estimate the charge transferred from one confined molecule. Thus, the CT either derived from DFT calculations or Raman measurements are displayed on figure 3 depending on the nature of the confined molecules. It is

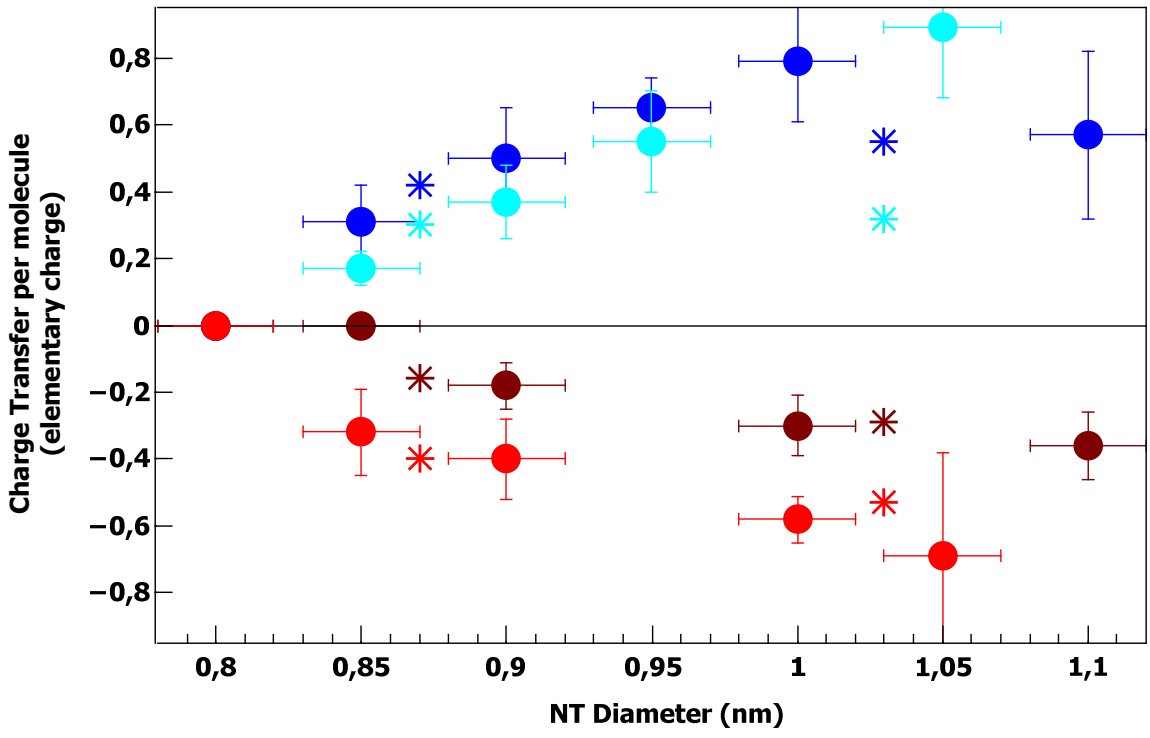

worth to mention that DFT calculations and Raman measurements are in very good agreement regarding the magnitude of the CT between the confined molecules and the host NT. These charge transfers experimentally evidenced or calculated clearly depend on the nanotube diameter.

Figure 3: *Charge transfer per molecule (part of elementary charge) between the confined molecules for 4T (blue circle), TMPD (cyan circle), TCNQ (brown) and F4TCNQ (red circle) and DFT claculations (star symbols).*

3.3 Fermi level shift

As a consequence of the CT, the Fermi level of NT should shift up or downwards depending on the nature (*n* or *p*-type) of the doping. Figure 4 exhibits the calculated Fermi level shift for the 4T@NT hybrid system as a function of the NT diameter. As observed for the CT in figure 3, the magnitude of the shift clearly increases with an increase of the NT diameter.

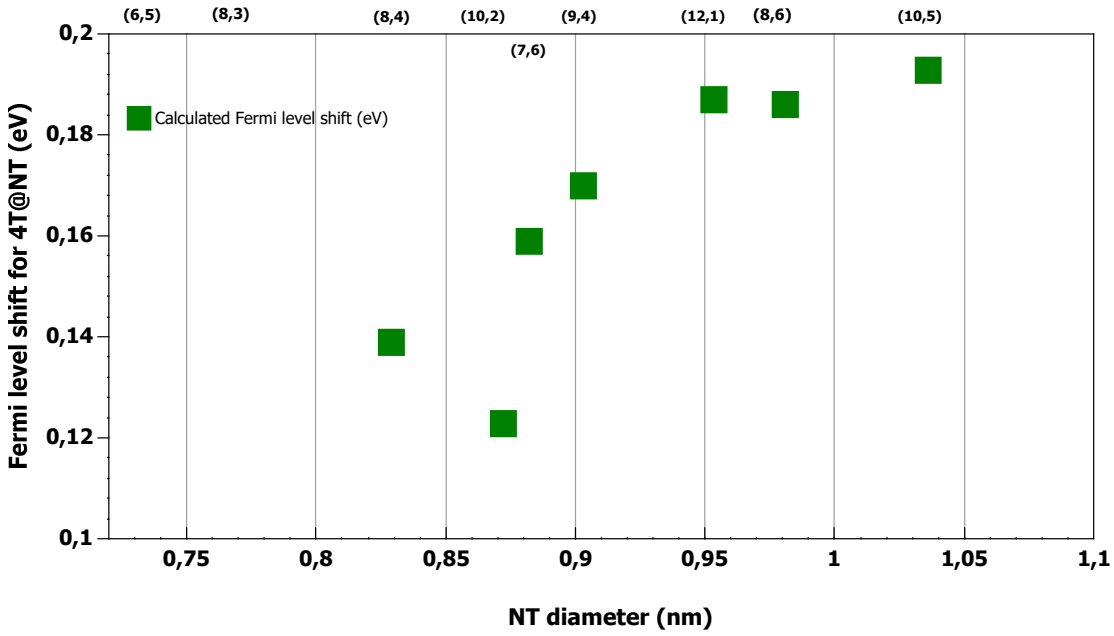

Figure 4: *Calculated Fermi level shift from DFT calculations upon 4T encapsulation*

Those results can be compared to macroscopic X-ray and ultraviolet photoemission spectroscopy measurements on NT assembly. Figure 5a shows the onset of the low energy secondary electron emission spectra, as previously reported.[45–47] Encapsulations of 4T and F_4TCNQ into the

hollow core of NT lead to shifts of 0.60 eV and 0.30 eV toward lower and higher binding energies, respectively. These changes in the UPS spectra allow us to suggest shifts in the Fermi level of the samples. Therefore, a downshift or an upshift in the Fermi level originates in a net increase of the low energy secondary electron emission spectrum, respectively. Finally, it is worth highlighting that minor changes in the work function of our samples might also be contributing to the changes in the onset of the low energy secondary electron emission spectra. Figure 5b shows the C 1s core-level spectra of the NT assemblies. It is important to remark that the presence of the molecules in the core of the NT notorious increased the FWHM of the C 1s peak (and implicitly of its components) when compared to empty NT samples. The Fermi level shifts exhibit the same trends using DFT and XPS/UPS measurements, confirming CT (electron or hole) and Fermi level shift (upward or downward) depending on the electron donor (or acceptor) character of the confined molecules. These results are summarized in table 1.

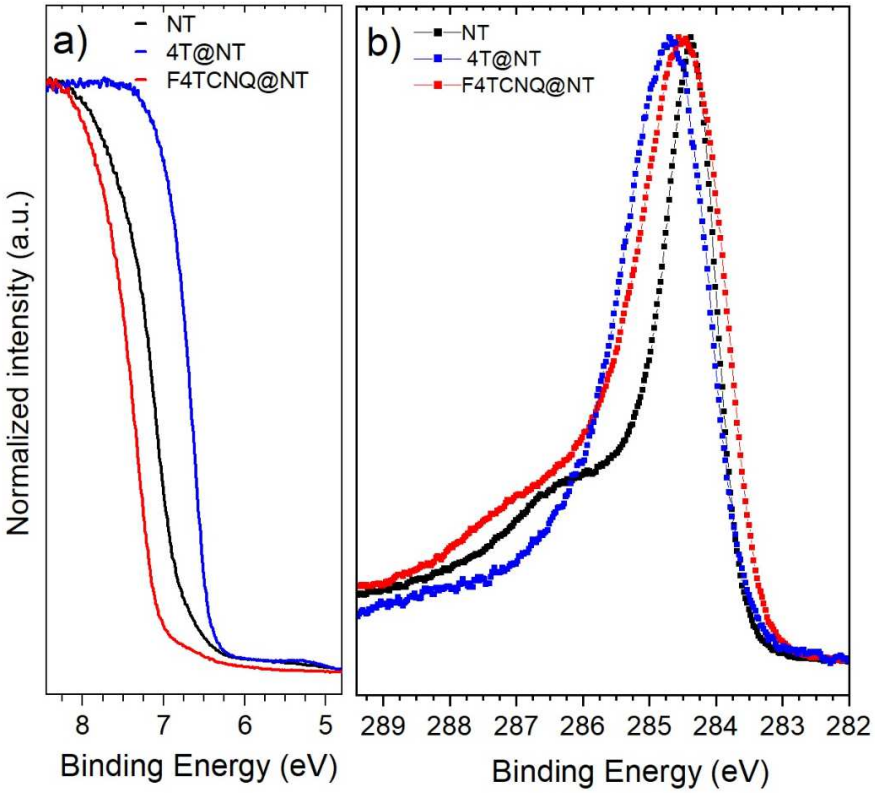

Figure 5: *a) UPS low energy secondary electron spectra of 4T@NT (blue), empty (black) and F_4TCNQ (red) are shown. The change in the work functions can be extracted from the onset shift of the low energy secondary electron spectra. b) C 1s X-ray photoemission spectra of 4T@NT (blue), empty (black) and F_4TCNQ (red). The experimental data are represented as dots, and the*

fitted data are represented as solid lines. For the fitting of the 4T@NT and F_4TCNQ spectra, an extra component is needed to acknowledge the contribution of the molecules to the C1s signal.

Table 1: *Fermi level shift from DFT calculations and UPS measurements.*

NT diameter	Method	4T@NT	F_4TCNQ@NT
≈0.9 nm	DFT	+0.19 eV	-0.16 eV
	UPS	+0.6 eV	-0.3 eV

3.4 Optical Properties

Photoluminescence properties of individual doped carbon nanotubes are studied. AFM and Raman polarization resolved measurements (figure 3, SM) are used to identify individual NT. Their PL spectra are investigated at 561 and 660 nm laser energies (Figure 6). Those energy excitation wavelengths correspond respectively to S_{22} transition of (6,5) (9,2) and (8,3) (7,5) (7,6) NT. PL spectra of isolated 4T@NT are given on figure 2. Significant enhancement of the PL intensity is evidenced after 4T encapsulation, especially for (9,2) (7,5) and (7,6) NT which show intensity ratios ($I_{4T@NT}/I_{NT}$) of 2.7 ± 1.3, 4.2 ±1.2 and 4.8 ±1 respectively.

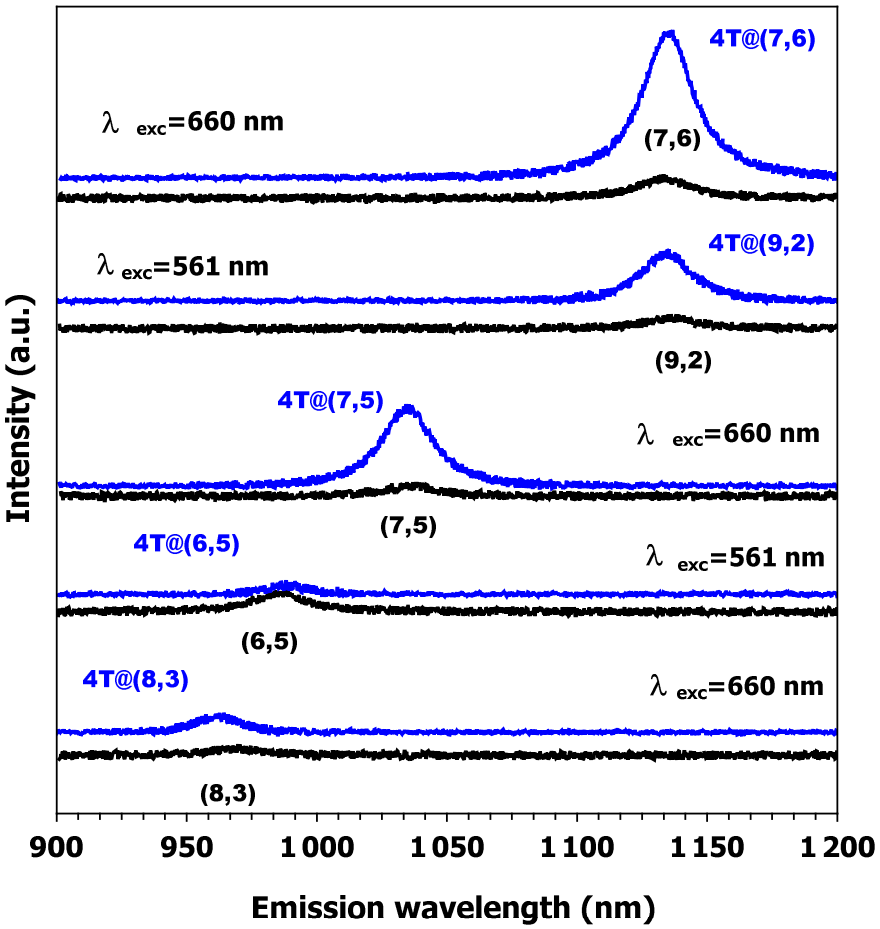

Figure 6: *Photoluminescence spectra of individual NT (black curve) and 4T@NT (blue curve) excited at 561 and 660 nm.*

For smaller NT as (8,3) and (6,5), PL ratios are 1±0.3 and 0.6 ± 0.4. Calculations suggest that hybrid structures with (8,3) and (6,5) NT are not stable, because those NT diameters are too small to accommodate 4T molecule, explaining that PL intensity remains unchanged (PL ratio ~1).

Same experiments were performed on individual hybrid F_4TCNQ@NT nanotube. No PL signal was detectable on a single object of any chirality. In order to go further and obtain a statistical average value of the PL intensity modifications over a large amount of hybrid NT, we performed macroscopic PL measurements. Near-infrared PL measurements allow a precise identification of semi-conducting NT chiral indexes.

Photoluminescence excitation (PLE) maps of empty NT (figure 7b) and functionalized with either electron donor (4T, figure 7a) or electron acceptor (F_4TCNQ, fig.7c) are displayed as a function of NT diameter.

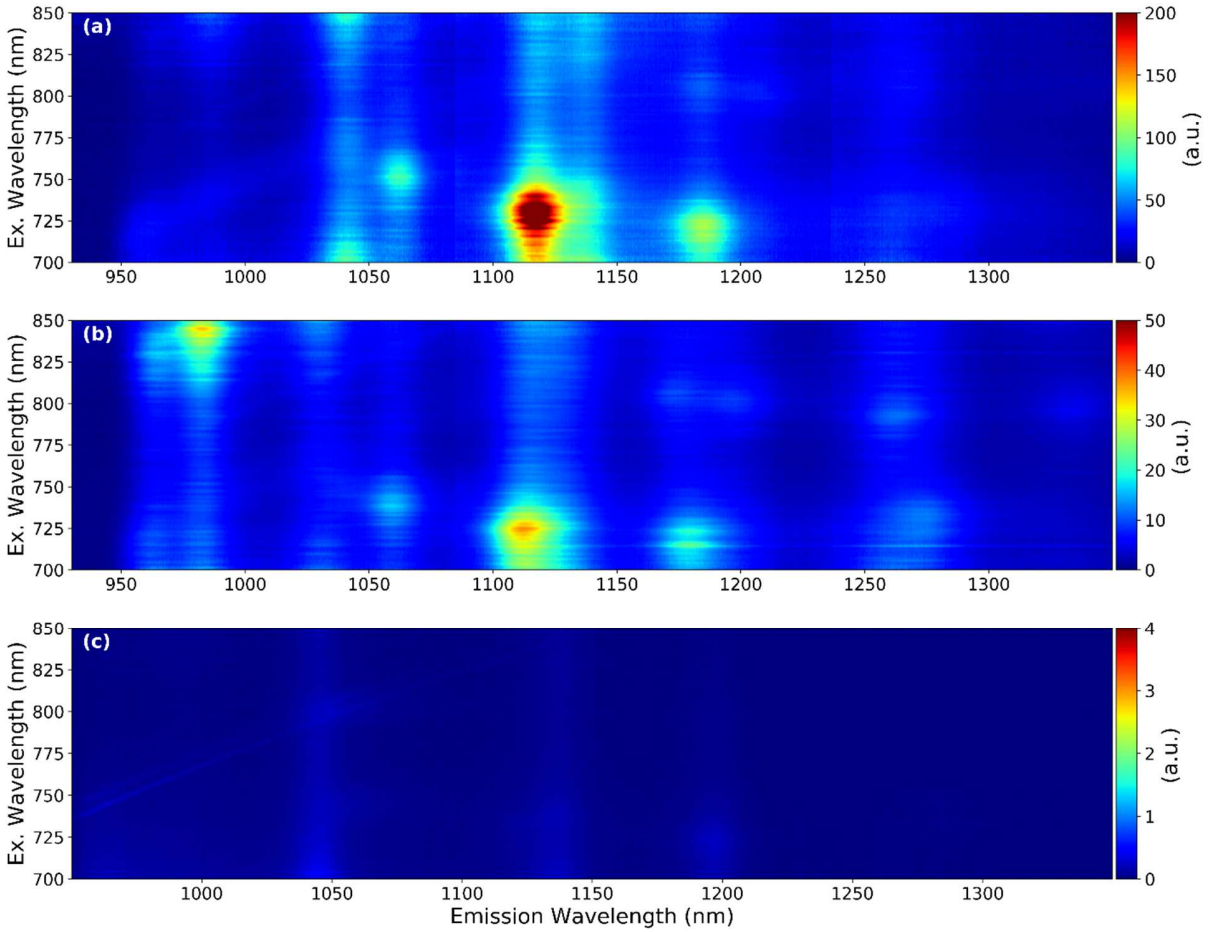

Figure 7*: PLE of 4T@NT(fig. 7a, top), empty NT (fig. 7b, middle), F_4TCNQ@NT(fig. 7c, down). Note that the intensity scales are not the same*

The significant enhancement of the PL intensity after 4T encapsulation observed on individual hybrid NT is confirmed together with the important drop after F_4TCNQ confinement, consistent with the quenching of the PL signal observed in isolated F_4TCNQ@NT. The modifications of the PL intensities are summarized in figure 8 which displays the PL intensity ratio (hybrid NT over empty NT) as a function of the NT diameter for the four molecules under investigations. It is worth mentioning that the magnitude of the enhancement or quenching after molecule encapsulation strongly depends on the NT diameter (Figure 8).

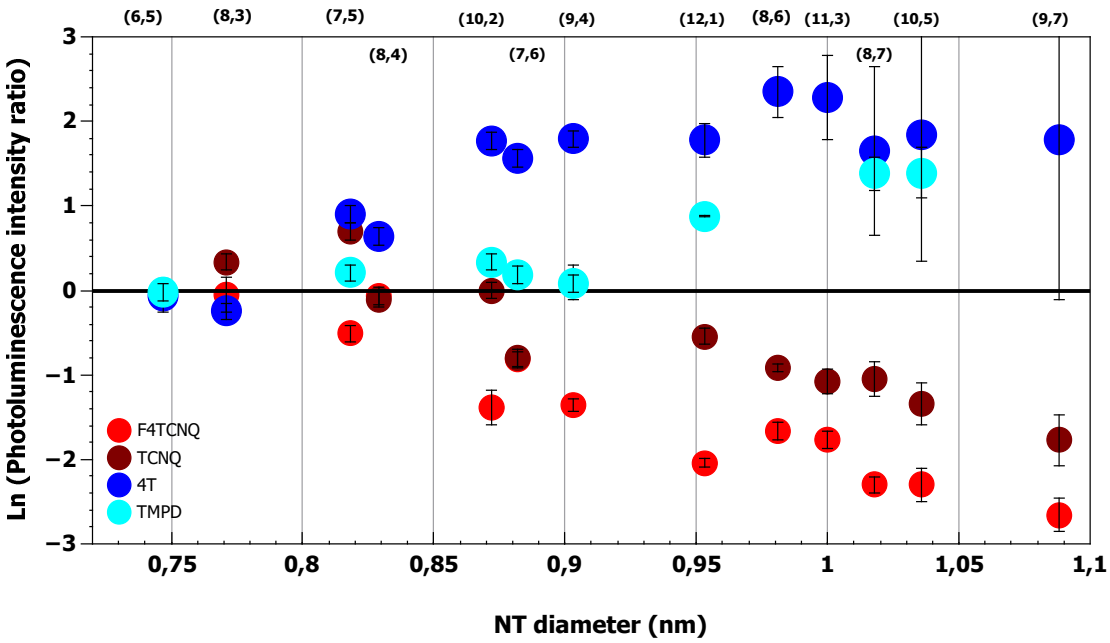

Figure 8: *Natural logarithm of PL intensity ratio (left scale) of 4T@NT (blue circle), TMPD@NT (cyan circle), TCNQ@NT (brown circle) and F_4TCNQ@NT (red circle) with respect to empty NT as a function of the NT diameter. Intensity ratio is the peak area ratio, calculated by systematically fitting the PL peak with a Lorentzian function and subtracting a background.*

4. Discussion

According to the electronic properties (ionization potential or electron affinity), electron (hole) transfer from the confined molecules to NT is expected for TMPD and 4T (respectively TCNQ and F_4TCNQ) with a more important magnitude of the CT for TMDP with respect to 4T (F_4TCNQ with respect to TCNQ). The charge transfers obtained by Raman spectroscopy and DFT calculations (figure 3) are consistent with these expectations, both qualitatively and quantitatively, except for 4T which seems to transfer slightly more than TMPD. This could be due to a weaker interaction between the TMPD molecule and the host nanotube. However, as the DFT calculations also predict this behavior, it is most likely that the ionization potential of the 4T molecules (estimated thanks to the sexithiophene molecule) is not accurately determined. Nevertheless, the ionization potential and electron affinities values of the different molecules and the nanotubes are relevant parameters to foresee qualitatively and quantitatively the CT between confined molecules and NT.

Another important point is that a clear dependence of the magnitude of the CT with the NT diameter is evidenced, both experimentally and theoretically (figure 3).

Concomitantly, the Fermi level up or downshift (figure 5 and table 1) is in good agreement with the electronic character (electron donor or acceptor) of the confined molecules. Once again, the NT diameter plays a very important role in the magnitude of the shift (at least from DFT calculations for 4T@NT). Therefore, the CT and the Fermi level shift are certainly governed by the molecule position inside the host NT, which strongly depends on the NT diameter.[14]

Finally, the PL intensity ratio (figure 8) follows a behavior closely related to those of the CT (figure 3) and then to the Fermi level position (as a charge transfer leads to a Fermi level shift). More precisely, for electron donor molecule (respectively electron acceptor) the PL intensity is significantly enhanced (respectively significantly quenched) whereas the Fermi level upshifts (respectively downshifts). In other words, a hole transfer leads to a PL quenching whose magnitude scales with the electron affinity of the molecules (the quenching is more important for F_4TCNQ than for TCNQ). For the electron donor molecules, the PL intensity enhancement is more important for the 4T@NT hybrid system than for the TMPD@NT hybrid systems, which is unlike the ionization potential we used but quite consistent with the CT measurements and calculations. One can therefore infer that there is a strong correlation between the PL intensity modifications and the Fermi level shifts (or the charge transfer).

The main assumption to account for this behavior is that narrow diameter NT are *p*-type doped because of curvature effects[48], but also due to oxygenated defects [49] and possibly adsorbed oxygen[50], leading to an intrinsically significant Fermi level shift. For instance, for NT with a diameter of around 1 nm, the *p*-type doping only due to curvature effects is evaluated at 0.03 hole per carbon atom,[48] corresponding to around four holes over a length of 2 nm (which corresponds roughly to a molecule length). Therefore, our narrow diameter NT are probably intrinsically “highly” p-doped, so that the Fermi level is not lying in the middle of the bandgap. These free holes can mediate a non-radiative Auger-type recombination[51] that substitute to radiative recombination [51–53], so that PL of NT is strongly reduced. Further *p*-doping with TCNQ and F_4TCNQ further downshifts the Fermi level, reducing more importantly the PL emission intensity. In contrast, electron doping of NT with 4T or TMPD (below one electron per molecule) shifts upwards the Fermi level, but without fully balancing out the intrinsic *p*-doping,

so that even after electron transfer, the hybrid NT are probably still *p*-type doped. However, as the hybrid NT is less *p* doped than the empty ones, radiative recombination is much more probable [23], favoring back PL emission.

CONCLUSIONS

Significant electron donation or withdrawal in hybrids NT is evidenced depending on the electronic character (electronic affinity or ionization energy) of the molecule confined into their hollow core. Spectroscopy (Raman, PL) at the single object scale allowed to measure CT and correlated PL intensity modifications. The Fermi level shift induced by CT is measured and calculated. All the results are consistent with a charge transfer from the confined molecule to the host nanotube, allowing to finely tune the Fermi level position and to monitor the photoluminescence emission intensity of the hybrid nanotube. The NT diameter is another relevant parameter to monitor the PL intensity.

ACKNOWLEDGEMENTS

Y.S. and K.S. acknowledge JSPS KAKENHI and JST-CREST, respectively, for financial support.

REFERENCES:

[1] Ulink college of Beijing, Z. Du, E. Choi, Ulink college of Beijing, B. Duanmu, Ulink college of Beijing, J. Warner, Ulink college of Beijing, A REVIEW ON CARBON NANOTUBE FIELD EFFECT TRANSISTORS, in: Recent Developments on Information and Communication Technology (ICT) Engineering, International Institute of Knowledge Innovation and Invention, Private; Limited (IIKII PTE LTD), 2019: pp. 143–146. https://doi.org/10.35745/icice2018v2.036.

[2] M. Salvato, M. Scagliotti, M. De Crescenzi, M. Crivellari, P. Prosposito, I. Cacciotti, P. Castrucci, Single walled carbon nanotube/Si heterojunctions for high responsivity photodetectors, Nanotechnology. 28 (2017) 435201. https://doi.org/10.1088/1361-6528/aa8797.

[3] N. Dhurandhar, P. Dwivedi, A Review Article on Carbon Nanotube Field Effect Transistors Technology, RJET. 8 (2019) 56–62. https://doi.org/10.30732/RJET.20190801007.

[4] C.-P. Lee, L.-Y. Lin, P.-Y. Chen, R. Vittal, K.-C. Ho, All-solid-state dye-sensitized solar cells incorporating SWCNTs and crystal growth inhibitor, J. Mater. Chem. 20 (2010) 3619. https://doi.org/10.1039/b925221e.

[5] X. He, H. Htoon, S.K. Doorn, W.H.P. Pernice, F. Pyatkov, R. Krupke, A. Jeantet, Y. Chassagneux, C. Voisin, Carbon nanotubes as emerging quantum-light sources, Nature Mater. 17 (2018) 663–670. https://doi.org/10.1038/s41563-018-0109-2.
[6] S. Ren, M. Bernardi, R.R. Lunt, V. Bulovic, J.C. Grossman, S. Gradečak, Toward Efficient Carbon Nanotube/P3HT Solar Cells: Active Layer Morphology, Electrical, and Optical Properties, Nano Lett. 11 (2011) 5316–5321. https://doi.org/10.1021/nl202796u.
[7] S. Cambré, W. Wenseleers, Separation and Diameter-Sorting of Empty (End-Capped) and Water-Filled (Open) Carbon Nanotubes by Density Gradient Ultracentrifugation, Angew. Chem. Int. Ed. 50 (2011) 2764–2768. https://doi.org/10.1002/anie.201007324.
[8] W. Wenseleers, S. Cambré, J. Čulin, A. Bouwen, E. Goovaerts, Effect of Water Filling on the Electronic and Vibrational Resonances of Carbon Nanotubes: Characterizing Tube Opening by Raman Spectroscopy, Adv. Mater. 19 (2007) 2274–2278. https://doi.org/10.1002/adma.200700773.
[9] N.V. Kurnosov, V.S. Leontiev, V.A. Karachevtsev, Enhancement of Photoluminescence from Semiconducting Nanotubes in Aqueous Suspensions due to Cysteine and Dithiothreitol Doping: Influence of the Sonication Treatment, Nanoscale Res Lett. 11 (2016) 490. https://doi.org/10.1186/s11671-016-1708-y.
[10] T. Shiraki, T. Shiraishi, G. Juhász, N. Nakashima, Emergence of new red-shifted carbon nanotube photoluminescence based on proximal doped-site design, Sci Rep. 6 (2016) 28393. https://doi.org/10.1038/srep28393.
[11] L. Alvarez, F. Fall, A. Belhboub, R. Le Parc, Y. Almadori, R. Arenal, R. Aznar, P. Dieudonné-George, P. Hermet, A. Rahmani, B. Jousselme, S. Campidelli, J. Cambedouzou, T. Saito, J.-L. Bantignies, One-Dimensional Molecular Crystal of Phthalocyanine Confined into Single-Walled Carbon Nanotubes, The Journal of Physical Chemistry C. 119 (2015) 5203–5210. https://doi.org/10.1021/acs.jpcc.5b00168.
[12] Y. Almadori, L. Alvarez, R. Le Parc, R. Aznar, F. Fossard, A. Loiseau, B. Jousselme, S. Campidelli, P. Hermet, A. Belhboub, A. Rahmani, T. Saito, J.-L. Bantignies, Chromophore Ordering by Confinement into Carbon Nanotubes, The Journal of Physical Chemistry C. 118 (2014) 19462–19468. https://doi.org/10.1021/jp505804d.
[13] S. Cambré, J. Campo, C. Beirnaert, C. Verlackt, P. Cool, W. Wenseleers, Asymmetric dyes align inside carbon nanotubes to yield a large nonlinear optical response, Nature Nanotechnology. 10 (2015) 248–252. https://doi.org/10.1038/nnano.2015.1.
[14] Y. Almadori, G. Delport, R. Chambard, L. Orcin-Chaix, A.C. Selvati, N. Izard, A. Belhboub, R. Aznar, B. Jousselme, S. Campidelli, P. Hermet, R. Le Parc, T. Saito, Y. Sato, K. Suenaga, P. Puech, J.S. Lauret, G. Cassabois, J.-L. Bantignies, L. Alvarez, Fermi level shift in carbon nanotubes by dye confinement, Carbon. 149 (2019) 772–780. https://doi.org/10.1016/j.carbon.2019.04.041.
[15] K. Yanagi, K. Iakoubovskii, S. Kazaoui, N. Minami, Y. Maniwa, Y. Miyata, H. Kataura, Light-harvesting function of β -carotene inside carbon nanotubes, Physical Review B. 74 (2006). https://doi.org/10.1103/PhysRevB.74.155420.
[16] E. Gaufrès, N.Y.-W. Tang, F. Lapointe, J. Cabana, M.-A. Nadon, N. Cottenye, F. Raymond, T. Szkopek, R. Martel, Giant Raman scattering from J-aggregated dyes inside carbon nanotubes for multispectral imaging, Nature Photonics. 8 (2013) 72–78. https://doi.org/10.1038/nphoton.2013.309.
[17] E. Gaufrès, N.Y.-W. Tang, A. Favron, C. Allard, F. Lapointe, V. Jourdain, S. Tahir, C.-N. Brosseau, R. Leonelli, R. Martel, Aggregation Control of α-Sexithiophene *via* Isothermal

Encapsulation Inside Single-Walled Carbon Nanotubes, ACS Nano. 10 (2016) 10220–10226. https://doi.org/10.1021/acsnano.6b05660.
[18] T. Takenobu, T. Takano, M. Shiraishi, Y. Murakami, M. Ata, H. Kataura, Y. Achiba, Y. Iwasa, Stable and controlled amphoteric doping by encapsulation of organic molecules inside carbon nanotubes, Nature Materials. 2 (2003) 683–688. https://doi.org/10.1038/nmat976.
[19] J. Campo, S. Cambré, B. Botka, J. Obrzut, W. Wenseleers, J.A. Fagan, Optical Property Tuning of Single-Wall Carbon Nanotubes by Endohedral Encapsulation of a Wide Variety of Dielectric Molecules, ACS Nano. 15 (2021) 2301–2317. https://doi.org/10.1021/acsnano.0c08352.
[20] K. Yanagi, Y. Miyata, H. Kataura, Highly Stabilized β-Carotene in Carbon Nanotubes, Advanced Materials. 18 (2006) 437–441. https://doi.org/10.1002/adma.200501839.
[21] R.S. Alencar, A.L. Aguiar, R.S. Ferreira, R. Chambard, B. Jousselme, J.-L. Bantignies, C. Weigel, S. Clément, R. Aznar, D. Machon, A.G. Souza Filho, A. San-Miguel, L. Alvarez, Raman resonance tuning of quaterthiophene in filled carbon nanotubes at high pressures, Carbon. 173 (2021) 163–173. https://doi.org/10.1016/j.carbon.2020.10.083.
[22] L. Alvarez, Y. Almadori, R. Arenal, R. Babaa, T. Michel, R. Le Parc, J.-L. Bantignies, B. Jousselme, S. Palacin, P. Hermet, J.-L. Sauvajol, Charge Transfer Evidence between Carbon Nanotubes and Encapsulated Conjugated Oligomers, The Journal of Physical Chemistry C. 115 (2011) 11898–11905. https://doi.org/10.1021/jp1121678.
[23] X. Liu, H. Kuzmany, P. Ayala, M. Calvaresi, F. Zerbetto, T. Pichler, Selective Enhancement of Photoluminescence in Filled Single-Walled Carbon Nanotubes, Advanced Functional Materials. 22 (2012) 3202–3208. https://doi.org/10.1002/adfm.201200224.
[24] K. Yanagi, K. Iakoubovskii, H. Matsui, H. Matsuzaki, H. Okamoto, Y. Miyata, Y. Maniwa, S. Kazaoui, N. Minami, H. Kataura, Photosensitive Function of Encapsulated Dye in Carbon Nanotubes, Journal of the American Chemical Society. 129 (2007) 4992–4997. https://doi.org/10.1021/ja067351j.
[25] S. Schäfer, N.M.B. Cogan, T.D. Krauss, Spectroscopic Investigation of Electrochemically Charged Individual (6,5) Single-Walled Carbon Nanotubes, Nano Lett. 14 (2014) 3138–3144. https://doi.org/10.1021/nl5003729.
[26] F. Yang, M. Wang, D. Zhang, J. Yang, M. Zheng, Y. Li, Chirality Pure Carbon Nanotubes: Growth, Sorting, and Characterization, Chem. Rev. 120 (2020) 2693–2758. https://doi.org/10.1021/acs.chemrev.9b00835.
[27] A. Belhboub, P. Hermet, L. Alvarez, R. Le Parc, S. Rols, A.C. Lopes Selvati, B. Jousselme, Y. Sato, K. Suenaga, A. Rahmani, J.-L. Bantignies, Enhancing the Infrared Response of Carbon Nanotubes From Oligo-Quaterthiophene Interactions, The Journal of Physical Chemistry C. 120 (2016) 28802–28807. https://doi.org/10.1021/acs.jpcc.6b09329.
[28] B. Kitiyanan, W.E. Alvarez, J.H. Harwell, D.E. Resasco, Controlled production of single-wall carbon nanotubes by catalytic decomposition of CO on bimetallic Co–Mo catalysts, Chemical Physics Letters. 317 (2000) 497–503.
[29] T. Mori, T. Kawamoto, Organic conductors—from fundamentals to nonlinear conductivity, Annu. Rep. Prog. Chem., Sect. C: Phys. Chem. 103 (2007) 134–172. https://doi.org/10.1039/B605647B.
[30] D. Mayevsky, J. Tosado, C.D. Easton, C.H. Ng, M.S. Fuhrer, B. Winther-Jensen, A simple technique for performing evaporation of quaterthiophene below the melting temperature for

vapour phase polymerisation and physical vapour deposition, RSC Adv. 5 (2015) 99806–99811. https://doi.org/10.1039/C5RA16897J.
[31] Y. Yoshida, Y. Kumagai, M. Mizuno, K. Isomura, Y. Nakamura, H. Kishida, G. Saito, Improved Dynamic Properties of Charge-Transfer-Type Supramolecular Rotor Composed of Coronene and F_4TCNQ, Crystal Growth & Design. 15 (2015) 5513–5518. https://doi.org/10.1021/acs.cgd.5b01138.
[32] D. Sanchez-Portal, P. Ordejon, E. Artacho, Jose.M. Soler, Density-functional method for very large systems with LCAO basis sets, International Journal of Quantum Chemistry. (1997) 453–461.
[33] J.P. Perdew, K. Burke, M. Ernzerhof, Generalized Gradient Approximation Made Simple, Physical Review Letters. 77 (1996) 3865–3868. https://doi.org/10.1103/PhysRevLett.77.3865.
[34] S. Grimme, Semiempirical GGA-type density functional constructed with a long-range dispersion correction, Journal of Computational Chemistry. 27 (2006) 1787–1799. https://doi.org/10.1002/jcc.20495.
[35] Y. Hirana, G. Juhasz, Y. Miyauchi, S. Mouri, K. Matsuda, N. Nakashima, Empirical Prediction of Electronic Potentials of Single-Walled Carbon Nanotubes With a Specific Chirality (n,m), Scientific Reports. 3 (2013). https://doi.org/10.1038/srep02959.
[36] N. Bendiab, A. Righi, E. Anglaret, J.L. Sauvajol, L. Duclaux, F. Béguin, Low-frequency Raman modes in Cs- and Rb-doped single wall carbon nanotubes, Chemical Physics Letters. 339 (2001) 305–310. https://doi.org/10.1016/S0009-2614(01)00351-7.
[37] M.V. Kharlamova, C. Kramberger, A. Mittelberger, K. Yanagi, T. Pichler, D. Eder, Silver Chloride Encapsulation-Induced Modifications of Raman Modes of Metallicity-Sorted Semiconducting Single-Walled Carbon Nanotubes, Journal of Spectroscopy. 2018 (2018) 1–9. https://doi.org/10.1155/2018/5987428.
[38] A. Das, A.K. Sood, Renormalization of the phonon spectrum in semiconducting single-walled carbon nanotubes studied by Raman spectroscopy, Physical Review B. 79 (2009). https://doi.org/10.1103/PhysRevB.79.235429.
[39] A. Das, A.K. Sood, A. Govindaraj, A.M. Saitta, M. Lazzeri, F. Mauri, C.N.R. Rao, Doping in Carbon Nanotubes Probed by Raman and Transport Measurements, Physical Review Letters. 99 (2007). https://doi.org/10.1103/PhysRevLett.99.136803.
[40] J.C. Tsang, M. Freitag, V. Perebeinos, J. Liu, Ph. Avouris, Doping and phonon renormalization in carbon nanotubes, Nature Nanotechnology. 2 (2007) 725–730. https://doi.org/10.1038/nnano.2007.321.
[41] S. Piscanec, M. Lazzeri, J. Robertson, A.C. Ferrari, F. Mauri, Optical phonons in carbon nanotubes: Kohn anomalies, Peierls distortions, and dynamic effects, Physical Review B. 75 (2007). https://doi.org/10.1103/PhysRevB.75.035427.
[42] H. Farhat, H. Son, Ge.G. Samsonidze, S. Reich, M.S. Dresselhaus, J. Kong, Phonon Softening in Individual Metallic Carbon Nanotubes due to the Kohn Anomaly, Physical Review Letters. 99 (2007). https://doi.org/10.1103/PhysRevLett.99.145506.
[43] R. Saito, M. Hofmann, G. Dresselhaus, A. Jorio, M.S. Dresselhaus, Raman spectroscopy of graphene and carbon nanotubes, Advances in Physics. 60 (2011) 413–550. https://doi.org/10.1080/00018732.2011.582251.
[44] M. Lazzeri, F. Mauri, Nonadiabatic Kohn Anomaly in a Doped Graphene Monolayer, Physical Review Letters. 97 (2006). https://doi.org/10.1103/PhysRevLett.97.266407.

[45] S. Braun, W.R. Salaneck, M. Fahlman, Energy-Level Alignment at Organic/Metal and Organic/Organic Interfaces, Adv. Mater. 21 (2009) 1450–1472. https://doi.org/10.1002/adma.200802893.
[46] J.C. Moreno-López, O. Grizzi, M.L. Martiarena, E.A. Sánchez, Initial Growth of *N* , *N* ′-Bis(1-ethylpropyl)perylene-3,4,9,10-tetracarboxdiimide Films on Cu(100), J. Phys. Chem. C. 117 (2013) 11679–11685. https://doi.org/10.1021/jp402494j.
[47] H. Ishii, K. Sugiyama, E. Ito, K. Seki, Energy Level Alignment and Interfacial Electronic Structures at Organic/Metal and Organic/Organic Interfaces, (n.d.) 21.
[48] A. Rakitin, C. Papadopoulos, J.M. Xu, Carbon nanotube self-doping: Calculation of the hole carrier concentration, Physical Review B. 67 (2003). https://doi.org/10.1103/PhysRevB.67.033411.
[49] G. Gordeev, A. Setaro, M. Glaeske, S. Jürgensen, S. Reich, Doping in covalently functionalized carbon nanotubes: A Raman scattering study: Doping in covalently functionalized carbon nanotubes, Physica Status Solidi (b). 253 (2016) 2461–2467. https://doi.org/10.1002/pssb.201600636.
[50] Y. Ohno, S. Kishimoto, T. Mizutani, Photoluminescence of single-walled carbon nanotubes in field-effect transistors, Nanotechnology. 17 (2006) 549–555. https://doi.org/10.1088/0957-4484/17/2/035.
[51] J.M. Kinder, E.J. Mele, Nonradiative recombination of excitons in carbon nanotubes mediated by free charge carriers, Phys. Rev. B. 78 (2008) 155429. https://doi.org/10.1103/PhysRevB.78.155429.
[52] V. Perebeinos, P. Avouris, Phonon and Electronic Nonradiative Decay Mechanisms of Excitons in Carbon Nanotubes, Phys. Rev. Lett. 101 (2008) 057401. https://doi.org/10.1103/PhysRevLett.101.057401.
[53] S. Yasukochi, T. Murai, S. Moritsubo, T. Shimada, S. Chiashi, S. Maruyama, Y.K. Kato, Gate-induced blueshift and quenching of photoluminescence in suspended single-walled carbon nanotubes, Phys. Rev. B. 84 (2011) 121409. https://doi.org/10.1103/PhysRevB.84.121409.

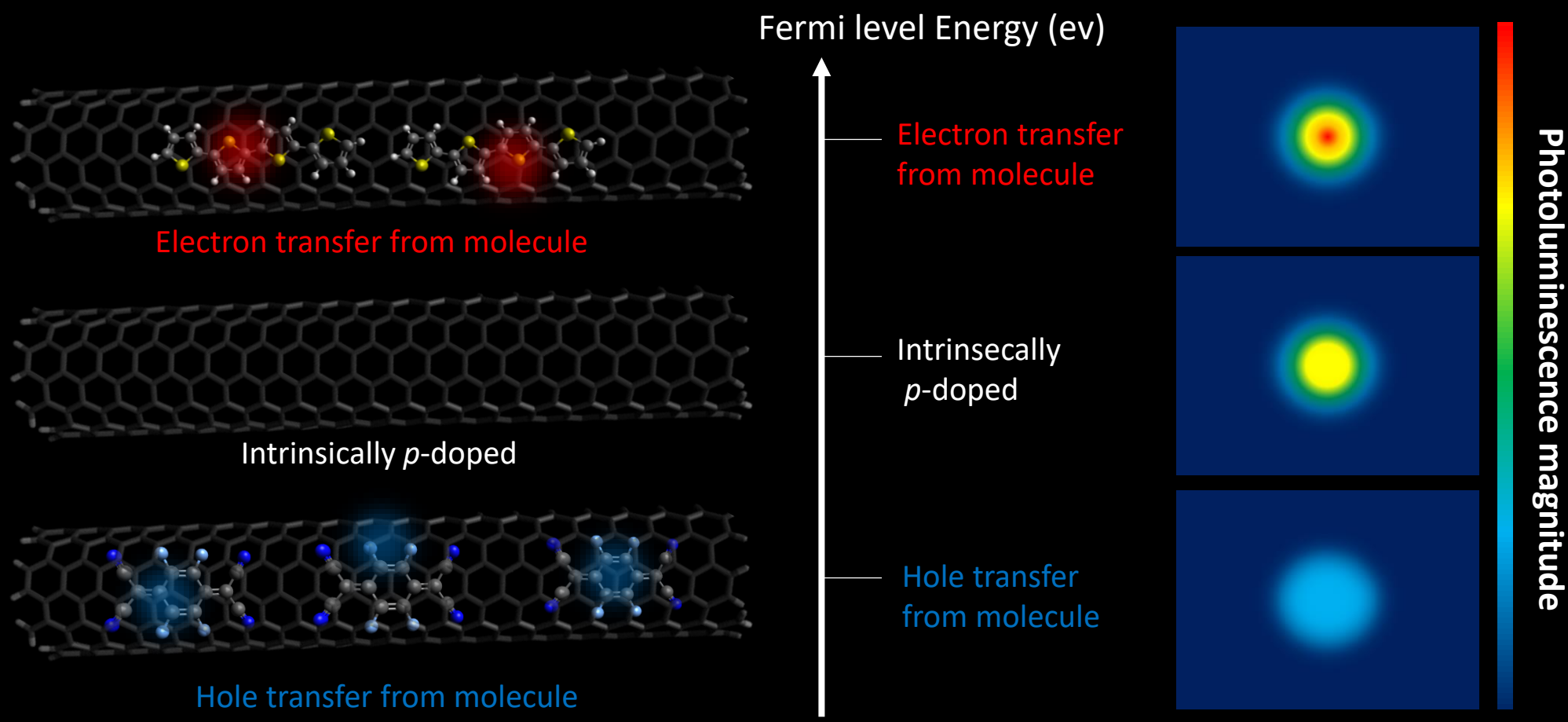
Electron transfer from molecule
Intrinsically p-doped
Hole transfer from molecule
Fermi level Energy (ev)
Electron transfer from molecule
Intrinsecally p-doped
Hole transfer from molecule
Photoluminescence magnitude